Environmental Science & Technology

pubs.acs.org/est

Article

Coupled Aerobic Methane Oxidation and Arsenate Reduction Contributes to Soil-Arsenic Mobilization in Agricultural Fields

Ling-Dong Shi, Yu-Jie Zhou, Xian-Jin Tang, Andreas Kappler, Ludmila Chistoserdova, Li-Zhong Zhu, and He-Ping Zhao*

Cite This: *Environ. Sci. Technol.* 2022, 56, 11845−11856

Read Online

ACCESS | Metrics & More | Article Recommendations | Supporting Information

ABSTRACT: Microbial oxidation of organic compounds can promote arsenic release by reducing soil-associated arsenate to the more mobile form arsenite. While anaerobic oxidation of methane has been demonstrated to reduce arsenate, it remains elusive whether and to what extent aerobic methane oxidation (aeMO) can contribute to reductive arsenic mobilization. To fill this knowledge gap, we performed incubations of both microbial laboratory cultures and soil samples from arsenic-contaminated agricultural fields in China. Incubations with laboratory cultures showed that aeMO could couple to arsenate reduction, wherein the former bioprocess was carried out by aerobic methanotrophs and the latter by a non-methanotrophic bacterium belonging to a novel and uncultivated representative of *Burkholderiaceae*. Metagenomic analyses combined with metabolite measurements suggested that formate served as the interspecies electron carrier linking aeMO to arsenate reduction. Such coupled bioprocesses also take place in the real world, supported by a similar stoichiometry and gene activity in the incubations with natural paddy soils, and contribute up to 76.2% of soil-arsenic mobilization into pore waters in the top layer of the soils where oxygen was present. Overall, this study reveals a previously overlooked yet significant contribution of aeMO to reductive arsenic mobilization.

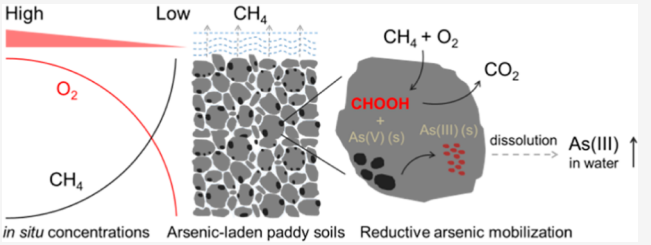

KEYWORDS: *arsenate reduction, aerobic methane oxidation, formate, arsenic mobilization, global distribution*

INTRODUCTION

Arsenic (As) is one of the most prevalent environmental poisons and carcinogens able to cause serious health issues[1,2] and ubiquitously distributed in Earth's atmosphere, hydrosphere, and pedosphere.[3−5] Mobilization of arsenic from soils and sediments into waters is generally mediated by reductive dissolution of As-bearing iron and/or manganese (oxyhydr)oxide minerals.[6−9] In addition to this, microbial reduction of arsenate [As(V)] to the more mobile arsenite [As(III)] is another important pathway for releasing the bio-unavailable, solid-associated arsenic into aquatic environments, with the requirement of oxidation of organic compounds including acetate, lactate, and humic substances.[10−13] Recently, naturally widespread methane (CH_4) was found to drive reductive arsenic mobilization by coupling anaerobic oxidation of methane (AOM) to arsenate reduction.[14] However, both arsenic and methane are also abundant in (hyp)oxic environments, for example, in groundwaters,[5,15−17] making it elusive whether and to what extent aerobic methane oxidation (aeMO) may influence arsenic release, with implications for global arsenic cycling and environmental contamination.

aeMO is carried out by several bacterial lineages belonging to Proteobacteria and Verrucomicrobia.[18,19] These methanotrophs routinely possess an oxygen-dependent methane monooxygenase (MMO) to catalyze the conversion of methane to methanol.[20,21] Despite the more favorable thermodynamics for oxygen reduction, aeMO can indeed support reduction of many other electron acceptors under hypoxic conditions, such as nitrate,[22−24] chromate,[25] and ferric iron,[26] which were observed in either axenic cultures or microbial communities. These observations, along with the comparable thermodynamic favorableness, suggest that aeMO could also be potentially coupled to arsenate reduction (aeMO-AsR).

Given that aerobic methanotrophs themselves are incapable of arsenate reduction, such a coupled process would require some oxygen for the methanotrophs to activate methane, along with a source of electrons for arsenate reduction by partner non-methanotrophs. Two potential sources of electrons that were previously proposed to function as electron carriers between these two physiological groups of organisms could be methane-derived methanol or formate (eqs 1−6).[27−30]

Methane oxidation to methanol

Received: March 16, 2022
Revised: July 16, 2022
Accepted: July 20, 2022
Published: August 3, 2022

$$CH_4 + 0.5O_2 = CH_3OH,\ \Delta G^0 = -116.1\ kJ\ mol^{-1}\ CH_4 \quad (1)$$

Methanol-based arsenate reduction

$$3HAsO_4^{2-} + CH_3OH + 5H^+ = 3H_3AsO_3 + HCO_3^- + H_2O,\ \Delta G^0 = -435.9\ kJ\ mol^{-1}\ CH_3OH \quad (2)$$

Methanol-linked overall reaction

$$3HAsO_4^{2-} + CH_4 + 0.5O_2 + 5H^+ = 3H_3AsO_3 + HCO_3^- + H_2O,\ \Delta G^0 = -552.0\ kJ\ mol^{-1}\ CH_4 \quad (3)$$

Methane oxidation to formate

$$CH_4 + 1.5O_2 = HCOO^- + H_2O + H^+,\ \Delta G^0 = -537.6\ kJ\ mol^{-1}\ CH_4 \quad (4)$$

Formate-based arsenate reduction

$$HAsO_4^{2-} + HCOO^- + 2H = H_3AsO_3 + HCO_3^-,\ \Delta G^0 = -162.0\ kJ\ mol^{-1}\ HCOOH \quad (5)$$

Formate-linked overall reaction

$$HAsO_4^{2-} + CH_4 + 1.5O_2 + H^+ = H_3AsO_3 + HCO_3^- + H_2O,\ \Delta G^0 = -699.6\ kJ\ mol^{-1}\ CH_4 \quad (6)$$

AOM coupled to arsenate reduction

$$4HAsO_4^{2-} + CH_4 + 7H^+ = 4H_3AsO_3 + HCO_3^- + H_2O,\ \Delta G^0 = -478.2\ kJ\ mol^{-1}\ CH_4 \quad (7)$$

As shown in theoretical thermodynamic equations, aeMO-AsR can produce more energy than the reported AOM-based arsenate reduction process when reacting 1 mol of methane (eqs 3, 6, and 7). We therefore hypothesized that in the co-presence of methane, oxygen, and arsenate, aeMO may take place and promote the arsenic release by coupling it to arsenate reduction, with a methane-derived organic compound as the electron carrier. To this end, we performed microcosm incubations for both laboratory cultures and field samples, uncovering a novel synergistic pathway of aeMO coupled to arsenate reduction and its previously overlooked yet significant contribution to global arsenic release.

MATERIALS AND METHODS

Collection of Laboratory Cultures and Field Samples. Since arsenic locates in the same group as antimony in the periodic table of elements, a microbial community from a previous antimonate-reducing bioreactor was used to enrich for arsenate-reducing microbes using a similar membrane biofilm batch reactor.[31] Methane was used as the sole electron donor, permeating from the lumen of hollow fibers. The arsenate concentration was set at 140 μM initially and replenished once consumed below 10 μM. The components of the medium were the same as previously described.[32] The medium was degassed using argon to keep the dissolved oxygen at ~1.0 mg/L.

Field samples were donated by Prof. Fang-Jie Zhao at Nanjing Agricultural University. Briefly, the samples were collected from the top layer of paddy soils distributed in Southern China during 2014 and 2021. These paddy fields are contaminated by arsenic and known to contain methane. Details can be found in Table S1.

Stoichiometry of Aerobic Methane Oxidation Coupled to Arsenate Reduction. Approximately 20 mL of the enrichment culture from the arsenate-reducing bioreactor was inoculated into 120 mL serum bottles. Then 60 mL of autoclaved mineral medium was introduced, along with the stock solution of arsenate to make the initial concentration at ~60 μM. Arsenate was replenished by adding the stock solution once its concentration decreased below 5 μM. The medium was degassed using argon for 5 min, leading the initial dissolved oxygen at ~1.0 mg/L, measured using an oxygen electrode (Starter 300D, OHAUS). All the bottles were tightly closed and sealed with butyl rubber stoppers and crimped aluminum caps, respectively. Finally, 10 mL of ^{13}C-labeled CH_4 was injected to the ratio of 20% (v/v) in the headspace as the sole electron donor. The bottles were incubated upside down in a dark shaker at 30 °C, with rotation at 150 rpm. Each experiment was carried out in triplicate. For the control setups, either only arsenate or only methane or none was added, following the same incubation protocol above.

Liquid samples were taken every day and immediately filtered through 0.22 μm membranes for the downstream measurement of arsenate, arsenite, and ^{13}C-labeled dissolved $^{13}CO_2$ (i.e., $^{13}CO_2 + {}^{13}HCO_3^- + {}^{13}CO_3^{2-}$). Gas samples were also taken over time to measure ^{13}C-labeled gaseous CO_2 in the headspace. The term $^{13}CO_2$ was used to indicate the total quantity of generated $^{13}CO_2$, both emitted into the headspace and dissolved in the liquid, after normalization by the total medium volume.

Inhibition Test of Methane Oxidation Coupled to Arsenate Reduction. Acetylene (C_2H_2) and 2-bromoethanesulfonate (BES) were used to specifically inhibit the activity of MMO[33] and methyl-coenzyme M reductase (MCR),[34,35] the key enzymes of aeMO and AOM, respectively. C_2H_2 was injected into the serum bottles to the final concentrations of 0.15 or 0.5 mM in the headspace. BES was added into the medium wherein the concentration was 20 or 50 mM. The setup with no inhibitors was used as a positive control, while a setup using the autoclaved enrichment culture served as a negative control. Other conditions were same as above. All experiments were run in triplicate.

Chemical Analyses. Arsenate was measured using ion chromatography configured with an AS19 column (Dionex ICS-1500, Thermo Scientific). Arsenite was first oxidized by 30% H_2O_2 and then quantified using the same instrument as above. Formate was measured using AS11 column-equipped ion chromatography. Gaseous $^{13}CO_2$ was measured by gas chromatography−mass spectrometry (GC 7890A coupled to MSD 5977B, Agilent), while the dissolved $^{13}CO_2$ was measured using isotope-ratio mass spectrometry (IR-MS, MAT 253, Thermo Scientific). At the end of incubation experiments, precipitates were centrifuged, washed, and freeze-dried. Energy-dispersive X-ray spectroscopy (Hitachi Se3400N

https://doi.org/10.1021/acs.est.2c01878
Environ. Sci. Technol. 2022, 56, 11845−11856

VP-SEM-EDS) was performed to characterize the elements in the precipitates, following the manufacturer's instructions.

Total As in soil field samples was measured by inductively coupled plasma mass spectrometry (ICP−MS) (NexION300XX, PerkinElmer) after a digestion with an acid mixture of HNO_3, HF, and H_2O_2 (volume ratio = 4/2/2), as described previously.[14] Pore waters were sampled by centrifuging for 10 min at 3100*g* and acidified by 6 M HCl to prevent arsenic transformation. Total Fe and Mn in pore waters were measured using the aforementioned ICP−MS. According to the textbook, the Mn(II) concentration in pore waters equals to the total Mn because only Mn(II) could be dissolved in the soil solution.[36] Fe(II) was determined by a spectrophotometric method using phenanthroline. As(III), As(V), dimethylarsinic acid [DMAs(V)], and monomethylarsinic acid [MMAs(V)] in pore waters were measured by high-performance liquid chromatography (HPLC) coupled to ICP−MS (NexION300XX, PerkinElmer) configured with an anion-exchange PRP X-100 HPLC column (250 × 4.1 mm I.D., 10 μm, Hamilton). Detailed methods could be found in our previous study.[14]

Extraction and Quantification of DNA and RNA. The biomass of lab cultures was collected at the beginning and end of the incubation with methane and arsenate and from the incubation with arsenate only as a control. DNA and RNA of the lab cultures were extracted using a PowerSoil DNA Isolation Kit and RNeasy PowerBiofilm Kit (Qiagen) following the manual. Soils were collected immediately at the end of the incubations inoculated with field samples and microcosm incubations. RNA of soils was extracted using a Soil RNA Kit (Omega) according to the instruction. The concentration and quality of extracted DNA and RNA were determined using a NanoDrop spectrophotometer (Thermo Scientific).

Reverse Transcription and Quantitative Polymerase Chain Reaction. Reverse transcription was performed by mixing reverse transcriptase, RNase inhibitor, random primer 6-mers, dNTP mixture, reaction buffer, and the RNA samples and reacting at 42 °C for 60 min, 70 °C for 15 min, and 4 °C, according to the reagent manual. The protocols of quantitative polymerase chain reaction (qPCR) were the same as described previously.[37] Briefly, primers 16SF (5′-GTGSTGCAYGGYTGTCGTCA-3′) and 16SR (5′-GTGSTGCAYGGYTGTCGTCA-3′) were used to quantify the bacterial 16S rRNA gene;[38] primers arrA-CVF1 (5′-CACAGCGCCATCTGCGCCGA-3′) and arrA-CVR1 (5′-CCGACGAACTCCYTGYTCCA-3′) were used to quantify the respiratory arsenate reductase gene *arrA*;[39] primers A189F (5′-GGNGACTGGGACTTCTGG-3′) and MB661R (5′-CCGGMGCAACGTCYTTACC-3′) were used to quantify the aeMO gene *pmoA*.[40] The concentration of target genes was calculated by comparing with the calibration curves which were produced from gene fragment-containing plasmids. The PCR efficiencies were 108.1, 91.2, and 112.6% for the bacterial 16S rRNA gene, *arrA*, and *pmoA*, respectively. All experiments were carried out in quadruplicates or triplicates. The probability (i.e., *p*-values) of differences between the two setups was calculated using the Mann−Whitney *U* test.

Metagenomic Sequencing and Analyses. The sequencing library of DNA samples was first constructed using an Illumina TruSeq DNA Nano Library Prep Kit and then sequenced using an Illumina HiSeq X Ten (2 × 150 bp). A total of 51.1 and 49.7 million reads were finally generated, of which 94.3% had the base call accuracy above 99.9% (Q30 score).

FastQC (http://www.bioinformatics.babraham.ac.uk/projects/fastqc/) was used to test the quality of the raw data. The low-quality reads were trimmed or removed by Trimmomatic using the default parameters.[41] Taxonomy of reads was classified using Kaiju (v 1.7.2).[42] The qualified reads were co-assembled into contigs by metaSPAdes.[43] Metabat was performed to bin the assembled contigs of which length longer than 500 bp,[44] and CheckM was further used to assess the quality of metagenome-assembled genomes (MAGs).[45] The BBmap package (https://sourceforge.net/projects/bbmap/) was applied to map the reads after quality control to assembled contigs to generate the relative abundance of MAGs. The taxonomy of MAGs was assigned using the toolkit GTDB-Tk according to the Genome Taxonomy Database (v 95).[46,47] Please note that only the taxonomies describing MAGs were according to the Genome Taxonomy Database; others in the present study were according to the NCBI Taxonomy Database.

MetaErg was employed to predict and annotate the open reading frames preliminarily.[48] Putative respiratory arsenate reductase was identified using HMMER (v 3.2.1) with a cutoff *e*-value $\leq 1 \times e^{-5}$ and a previously constructed hidden Markov model (HMM).[14,49] Extracted protein sequences were aligned with references of the bacterial molybdopterin reductase superfamily including recognized respiratory arsenate reductases by MUSCLE (v 3.8.1551).[50] The obtained alignment was used to produce the phylogenetic tree using IQ-TREE (v 1.6.12) with the standard model selection[51] to further validate the annotations. Proteins clustered with known arsenate reductase sequences were regarded as the potential arsenate reductases. The downstream sequences were extracted, aligned, and phylogenetically evaluated by comparing with recognized reference groups using the same procedure described above. Two potential arsenate reductase genes were located in the end of respective contigs and thus had no downstream content.

For identifying genes for MMO and the corresponding aerobic methanotrophic bacteria, similar procedures were carried out using the *pmoB* HMM (TIGR03079) downloaded from the TIGRFAMs database.[52] For identifying genes for MCR and the corresponding anaerobic methanotrophic archaea, the *mcrA* HMM (PF02249) downloaded from the Pfam database was used.[53]

The phylogeny of MAGs of interest was analyzed using a concatenated set of 120 bacterial-specific conserved marker genes.[54] Metabolic pathways in MAGs were recruited using MetaErg combined with GhostKOALA and BLAST.[48,55,56] The formate dehydrogenase of certain MAGs was phylogenetically analyzed as described for other proteins. The conserved features and sites of recovered proteins were identified based on the Conserved Domain Database (CDD).[57] The protein structures were modeled, predicted, and analyzed by the Phyre2 web portal.[58]

Comparison of Arsenate Reduction with Methane versus Formate. Given the eight and two electron equivalents from methane and formate (assuming the oxidation to CO_2), respectively, 2 mL of methane (0.09 mmol) and 4.5 mM of formate (3.6 mmol) were used as the sole electron donors in different batch incubations, both in excess of that required for complete reduction of arsenate to arsenite. The initial arsenate concentration was at approx-

https://doi.org/10.1021/acs.est.2c01878
Environ. Sci. Technol. 2022, 56, 11845−11856

imately 100 μM. Other conditions were the same as described in previous subsections, except for the inoculum amount of the enrichment culture. The rate of arsenate reduction was determined by fitting empirical data to a pseudo-zero-order equation. All the setups were in triplicate.

Incubations Inoculated with Field Samples. Approximately 0.3 g of dry soils sampled from paddy fields was incubated in 60 mL serum bottles, along with 30 mL of autoclaved mineral medium (Figure S1a). Again, the medium was degassed to maintain the dissolved oxygen at ~1.0 mg/L. After introducing ~120 μM of arsenate, all the bottles were tightly closed and sealed, followed by injecting 3 mL of ^{13}C-labeled CH_4 to a ratio of 10% (v/v) in the headspace. These bottles were incubated in a dark shaker at 25 °C upside down, with rotation at 150 rpm. Each experiment was carried out in triplicate. For the control setups, either only arsenate or only methane was added, following the above procedure. Protocols of sampling and measurements were the same as described for lab cultures in the preceding.

Microcosm Incubations Mimicking In Situ Conditions. Approximately 13.0 g of dry soils through a 10-mesh sieve was incubated in 60 mL serum bottles. Then 8.7 mL of autoclaved Milli-Q water was added with a 40% volumetric water content. Bottles were open initially to maintain (hyp)oxic conditions for the 10-day incubations and then sealed to establish a 10% (v/v) methane headspace by injecting 5 mL of ^{13}C-labeled CH_4. All the microcosms were incubated at 25 °C in a dark chamber and without shaking (Figure S1b), simulating the in situ conditions of paddy fields. In addition, two control setups were conducted, where one used argon to replace $^{13}CH_4$ and the other used autoclaved soils. Samples were taken at the beginning (day 0) and end (day 10) of the incubations for measuring target items. All the microcosm incubations were performed in triplicate.

Total soil-arsenic mobilization was measured from the biotic setup amended with $^{13}CH_4$. The contribution of abiotic physico-chemical desorption to total soil-arsenic mobilization was measured from the autoclaved setup. The contribution of aeMO-AsR was calculated by subtracting the released arsenite in the $^{13}CH_4$ setup from that in the argon setup. The contribution of other transformations was calculated by subtracting the released arsenite in the argon setup from that in the autoclaved setup.

Thermodynamic Calculations. The *CRC handbook of chemistry and physics* was referred for the values of Gibbs free energy of formation of substances.[59] The pH, temperature, and partial pressure were set as 7.0, 25 °C, and 1 atm, respectively, given their minor difference among the general environments considered and the resulting minor impact on thermodynamic calculation results. Calculations and corrections for each reaction were performed based on the previously reported protocols.[60] The thermodynamics of the overall reaction could be calculated by eliminating the intermediate formate.

To determine the thermodynamics of methane oxidation to formate, the concentrations of formate were assumed to be 1 nM, 1 μM, and 1 mM, with our experimentally measured value (~10 μM) included into this range. The actual environmental conditions were outlined according to (1) the reported minimum oxygen concentration for aeMO,[22] (2) the saturated dissolved oxygen concentration, and (3) the maximum methane dissolved in pore waters that we could find.[61] To determine the thermodynamics of formate oxidation coupled to arsenate reduction, the concentrations of arsenite were assumed to be 1 nM, 1 μM, and 1 mM, which included our experimentally measured value (~160 μM). The upper and lower limits of the actual environment were selected as 1 μg As/L and 75 mg As/L, respectively, according to the usually detected values in nature.[62] The bicarbonate concentration was set as 8.20 mM based on the reported average value.[63]

In our experiments depicted in Figure 1, the initial concentrations of dissolved oxygen, methane, formate, arsenate, and bicarbonate were measured as 31.25 μM (1 mg/L), 0.3125 mM (20%, v/v), 10.75 ± 1.06 μM, ~60 μM, and 4.92 mM, respectively. The dissolved arsenite concentration was selected as the maximum value (i.e., ~160 μM), which in theory was the most unfavorable for the reaction. We calculated the actual Gibbs free energy of the reactions by using these measured concentrations to correct the standard equations, following the accepted protocols.[60]

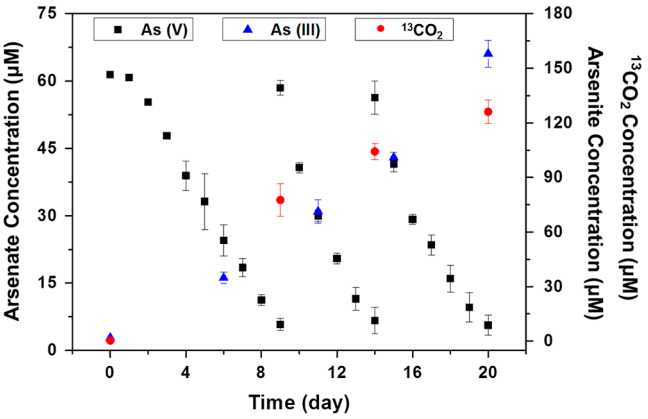

Figure 1. Arsenic transformation and DIC production by the arsenate-reducing microbial community. ^{13}C-labeled methane was injected into serum bottles as the sole electron donor. Arsenate was pulse-fed at days 0, 9, and 14. Please note the different *Y*-axis scales for arsenate, arsenite, and $^{13}CO_2$. Error bars indicate standard deviations of triplicate setups.

Global Distribution Inferred by Bio-Informatics. The co-distribution of different functional groups was identified by searching reference sequences against the non-redundant protein database of MGnify (2019.05) using Diamond (v 0.9.18) with a cutoff *e*-value of $1 \times e^{-5}$ and a more sensitive mode.[64,65] Matched protein sequences were linked to assemblies and samples, of which geographic information was extracted and plotted using R packages.

DATA AVAILABILITY

All the metagenomic sequencing data involved in the study have been submitted to the Sequence Read Archive, with the BioProject accession number of PRJNA698417.

RESULTS AND DISCUSSION

Aerobic Methane Oxidation Coupled to Arsenate Reduction in Laboratory Cultures. To explore the feasibility and physiological pathway of aeMO coupled to arsenate reduction, we first simplified the experimental system by inoculating a bioreactor with lab cultures that efficiently reduced another pnictogen, antimony,[66] and running it with methane and arsenate as the electron donor and acceptor, respectively, under hypoxic conditions. After 40 days of operation, reduction of arsenate was observed in the

https://doi.org/10.1021/acs.est.2c01878
Environ. Sci. Technol. 2022, 56, 11845−11856

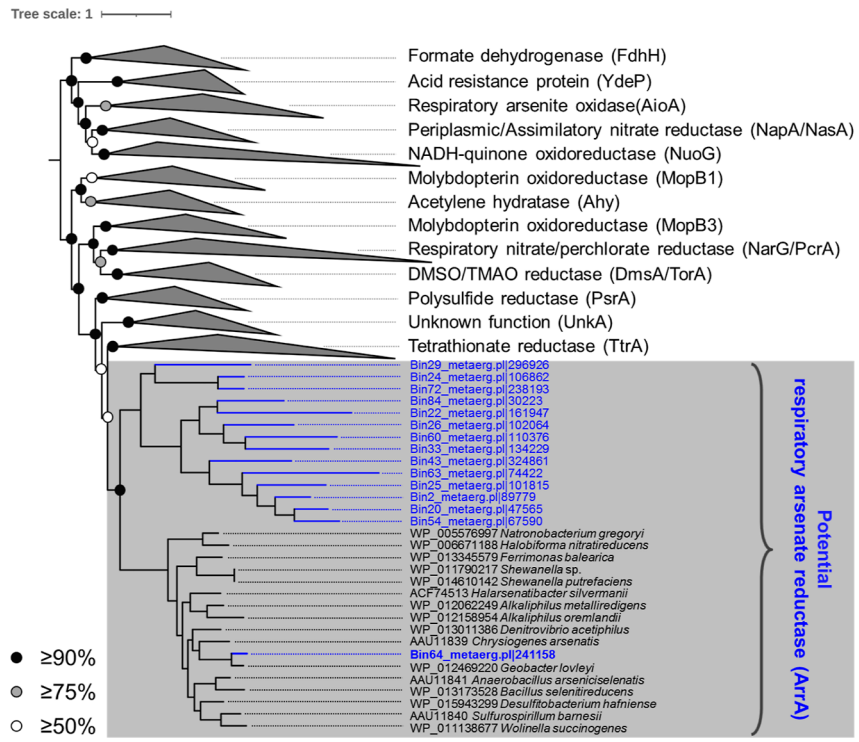

Figure 2. Phylogenetic tree of representative proteins of the bacterial molybdopterin reductase superfamily. Protein sequences highlighted by gray shadow indicate the potential respiratory arsenate reductases. Sequences identified in this study are shown in blue font. Circles of different colors indicate different bootstrap supports based on 1000 replicates. The scale bar represents amino acid changes.

constructed CH_4-based bioreactor (Figure S2). Batch tests inoculated from the established bioreactor demonstrated that approximately 60 μM of arsenate was reduced in 9 days when amended with ^{13}C-labeled CH_4. Another two pulse feeds of arsenate exhibited a similar reduction pattern (Figure 1). The arsenite content increased to ~160 μM accordingly, which was almost equal to the total decrease in arsenate (~158.3 μM) (Figure 1), showing a complete reduction of arsenate to arsenite, dissolved in the supernatant. This activity was further confirmed by energy-dispersive spectroscopy of bulk deposits with no remaining arsenic signal after reduction of As(V) to As(III) (Figure S3). In contrast, no arsenate reduction was observed with the same enrichment culture as the inoculum but in the absence of methane (Figure S4), suggesting the dependency of arsenate reduction on methane oxidation.

In the presence of both $^{13}CH_4$ and arsenate, ^{13}C-labeled CO_2 was produced continuously to ~125 μM (Figure 1). The amount of $^{13}CO_2$ was much higher than the theoretical value required for AOM coupled to arsenate reduction (i.e., 40 μM, according to eq 7), indicating that, most likely, aeMO was responsible for this process, rather than AOM.

To validate this hypothesis, specific inhibitors for aeMO (acetylene, C_2H_2) and AOM (2-bromoethanesulfonate, BES) were added to microcosm incubations at different concentrations.[33−35] The amendment of 0.15 mM or 0.5 mM C_2H_2 completely inhibited arsenate reduction, while BES addition, even as high as 50 mM, had no inhibitory effect (Figure S5). C_2H_2 and BES are known to efficiently inhibit, respectively, MMO, the oxygen-dependent enzyme key to aeMO, and MCR, the oxygen-independent enzyme key to both methanogenesis and AOM.[37,67,68] These results further supported our hypothesis that arsenate must be reduced in conjunction with aeMO, fueled by aerobic methanotrophic bacteria under hypoxic conditions. Contrary to the previously described AOM-dependent arsenate reduction driven by anaerobic methanotrophic archaea,[14] the process discovered here required trace oxygen for methane activation.[69] In general, oxygen is a more thermodynamically favorable electron acceptor than others like arsenate and selenate and thus can outcompete them for reduction.[70,71] Given the sufficient supply of the electron donor methane in hypoxic environments, coexisting arsenate could be reduced effectively after bulk oxygen was consumed to a certain level, as observed in methane-based nitrate and iron reductions.[22,26] Overall, we uncovered the not-yet-reported aeMO coupled to arsenate reduction using laboratory cultures.

Organisms and Genes Responsible for aeMO-AsR. To characterize the microbial community enabling aeMO-AsR, metagenomic sequencing was carried out at the beginning and the end of the arsenate incubation. Most metagenomic reads belonged to the bacteria domain, including the phyla Proteobacteria and Verrucomicrobia, which contain aerobic methanotrophic bacteria (Figure S6). Only a minor fraction (0.17−0.18%) of the reads belonged to Euryarchaeota, an archaeal phylum that contains taxa capable of AOM, likely suggesting a negligible contribution of AOM to arsenate reduction in the current study.

Read assembly and binning recovered a total of 67 MAGs of completeness >50%, with <10% contamination (Table S2). The relative abundances of several MAGs were increased to above 1% when amended with arsenate, for example, Bin.64, Bin.47, and Bin.3, all belonging to Proteobacteria; Bin.36 belonging to Bacteroidota; and Bin.20 belonging to Actinobacteriota (Figure S7). On one hand, a search for genes encoding MCR failed with no candidate genes identified. On the other hand, genes encoding the particulate MMO

https://doi.org/10.1021/acs.est.2c01878
Environ. Sci. Technol. 2022, 56, 11845−11856

(*pmoCAB*) were identified in several MAGs, which were classified as *Methylocystis* (Bin.58 and Bin.80), *Methylosinus* (Bin.48 and Bin.119), *Methylomonas* (Bin.14), and *Methylococcus* (Bin.87) (Figure S8 and Table S2). Together with the much higher transcriptional activity of *pmoA* in incubations amended with methane and arsenate (Figure S9), these data again supported the presence of aerobic methanotrophs in the arsenate-reducing microcosms and their key role in aeMO-AsR.

Over the incubation, bacterial 16S rRNA gene copy numbers increased significantly from $(2.25 \pm 0.34) \times 10^{12}$ to $(9.53 \pm 1.16) \times 10^{12}$ per liter (Mann−Whitney *U* test, $p = 0.029$; Figure S10). A control experiment with the same microbial community incubated without $^{13}CH_4$ and not active in reducing arsenate did not show a significant increase in bacterial 16S rRNA gene copy numbers (Mann−Whitney *U* test, $p = 0.886$), suggesting that the presence of both arsenate and methane promoted the growth of bacteria. The likelihood of arsenate being reduced via the respiration pathway was further confirmed by the significant elevation of both gene copies for respiratory arsenate reductase (*arrA*) and the ratio of *arrA* to the 16S rRNA gene, with the former increasing from $(2.38 \pm 0.05) \times 10^{10}$ to $(3.85 \pm 0.39) \times 10^{11}$ copies/L and the latter increasing from 1.06 to 4.04% (Figure S10). Additionally, the transcription of *arrA* was much higher in the co-presence of methane and arsenate than in the control setup (Figure S9), validating its activity in aeMO-AsR further.

Among the predicted coding sequences, putative *arrA* genes were recovered and used to construct a phylogenetic tree along with the known enzymes belonging to the microbial molybdoreductase superfamily. A total of 15 candidates were clustered with the large subunit of the known arsenate reductases (ArrA) and thus identified as potential respiratory arsenate reductase genes (Figure 2). In addition to genes for the large catalytic subunit, genes for the potential small, iron-sulfur subunit (ArrB) were also identified and phylogenetically characterized.[72] Among the 13 candidate homologs of ArrB identified, only one, from Bin.64, clustered with the reference sequence for the iron-sulfur subunit of arsenate reductase, while the rest formed a separate cluster of uncharacterized proteins (Figure S11). Therefore, the gene operon belonging to Bin.64 was inferred to be responsible for the methane-dependent arsenate reduction.

The topology of the putative active molybdopterin cofactor binding sites of the recovered ArrA sequence conformed to those of the canonical respiratory arsenate reductases (Figure S12), along with the modeled fold structure that was identical to that of the arsenate reductase of *Shewanella* sp. ANA-3 (ident = 49%, confidence = 100%).[73] These data support the role of a bacterium represented by Bin.64, classified as a member of *Burkholderiaceae* (Table S2), in arsenate reduction. Accordingly, the relative abundance of Bin.64 increased dramatically from 7.41 to 16.56% over the course of the incubation experiment. Taken together, through metagenomic analyses, we identified the organisms likely to be involved in aeMO and respiratory arsenate reduction, respectively, that is, aerobic methanotrophs belonging to several genera and a member of *Burkholderiaceae*.

Potential Electron Carriers Involved in aeMO-AsR. Despite the high completeness of aerobic methanotrophs and potential arsenate reducers (all >90% except for a methanotrophic bacterium Bin.48 of 60.06%, Table S2), the former group members involved in methane-dependent arsenate reduction encode no functions for arsenate reduction, and the latter, represented by Bin.64, does not encode methane oxidation functions. Therefore, we hypothesized that these organisms must act in synergy and thus likely share a metabolite to serve as an electron carrier. Based on the stoichiometry of methane oxidation/arsenate reduction (Figure 1), the ratio of arsenate removal to $^{13}CO_2$ production was 1.26, closer to the theoretical value of formate as an intermediate for aeMO-AsR (i.e., 1.0, eq 6) than other products (e.g., methanol, eq 3). In support of this hypothesis, the average rate of arsenate reduction fed with formate (1.98 ± 0.12 μM/h) was much higher than that with methane (0.79 ± 0.03 μM/h) in batch tests, demonstrating that formate was the preferred electron donor for arsenate reduction (Figure S13). Indeed, formate accumulation was measured in the medium at 10.75 ± 1.06 μM when only methane but not arsenate was present, while formate was undetectable in the presence of both methane and arsenate as well as when both methane and arsenate were absent (<2 μM). These results suggested the rapid utilization of formate in conjunction with arsenate reduction (Figure S13). Accordingly, the proposed arsenate respirer, represented by Bin.64, possesses a canonical formate dehydrogenase that could be responsible for formate oxidation (Figure S14). Based on these data, we propose that as part of the aeMO-AsR pathway, (bacterial) aerobic methanotrophs oxidize methane and excrete formate, which is used as an interspecies electron carrier for arsenate reduction by *Burkholderiaceae* (Figure 3).

The released formate appeared to support other community members, of which relative abundances increased to >1% during the microcosm incubation (Figure S7 and Table S2). Canonical formate dehydrogenases, along with cytochrome cbb_3 and *bd* type oxidases, were encoded by these organisms (Bin.3, Bin.20, Bin.36, Bin.9, Bin.47, and Bin.90), apparently supporting their dominance in the aeMO-AsR community, under hypoxic conditions (Figures 3 and S15).

Overall, reaction stoichiometry, metagenomic analyses, and metabolite measurements all support a synergistic nature of methane-dependent arsenate reduction, carried out by the aerobic methanotrophs and members of *Burkholderiaceae*, with formate as the interspecies electron carrier. Formate is well known to support methanogenesis-based syntrophy[74−76] and was demonstrated to mediate the methane-oxidation-based selenate reduction recently.[77] The present study provides another clear example for formate coupling aeMO to the reduction of oxides, highlighting the possibility that similar trophic relationships may link methane metabolism to a range of terminal electron acceptors in (hyp)oxic environments.

Arsenic Release from aeMO-AsR in the Real World. To test the existence of aeMO-AsR in nature, field samples were collected from paddy soils containing both methane and arsenic across southern China (Table S1). Ex situ incubations inoculated with soil samples showed varying degrees of methane oxidation (indicated by $^{13}CO_2$ production after $^{13}CH_4$ amendment) and arsenate reduction (Figure S15). Partial occurrence of these biochemical processes in microbial setups without external addition of $^{13}CH_4$ or As(V) was fueled by indigenous organic matter present in the soils functioning as an electron donor for As(V) reduction or by residual oxygen in the medium functioning as an electron acceptor for methane oxidation (Table S1).[9,78] However, incubations together with $^{13}CH_4$ and As(V) significantly enhanced both arsenate reduction and methane oxidation (Figure 4), suggesting that

https://doi.org/10.1021/acs.est.2c01878
Environ. Sci. Technol. 2022, 56, 11845−11856

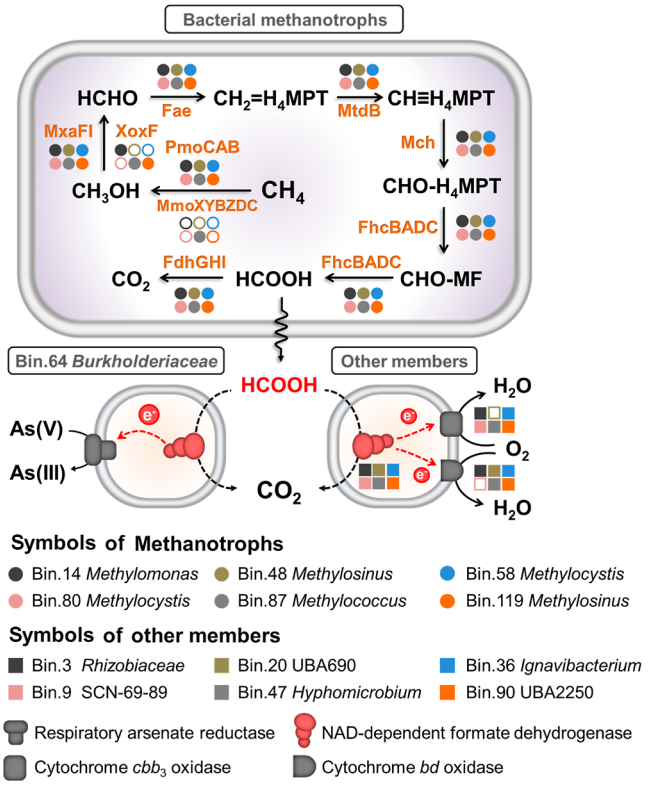

Figure 3. Proposed synergistic pathway coupling aeMO to arsenate reduction and oxygen respiration. Different symbols and colors represent different community members. Filled symbols indicate the existence of genes, while blank ones indicate no genes in the corresponding MAGs. Abbreviations: Pmo, particulate methane monooxygenase; Mmo, soluble methane monooxygenase; Mxa, calcium-dependent methanol dehydrogenase; Xox, lanthanide-dependent methanol dehydrogenase; Fae, formaldehyde activating enzyme; Mtd, methylene tetrahydromethanopterin dehydrogenase; Mch, methenyl tetrahydromethanopterin cyclohydrolase; Fhc, formyltransferase/hydrolase complex; Fdh, NAD-dependent formate dehydrogenase.

field samples have the potential for aeMO-AsR. In support of this, the key genes of respiratory arsenate reductase (*arrA*) and particulate MMO (*pmoA*) were transcriptionally active, with 1.5×10^7–1.36×10^8 and 2.6×10^7–8.3×10^8 transcript copies per gram dry soil, respectively. Gene transcriptions had significantly positive correlations with the corresponding biochemical processes, further validating the activity of aeMO-AsR in field samples (Figure 4). The ratio of arsenate reduction to aeMO was 1.32 ± 0.22 ($n = 8$), which was close to the value observed in lab cultures, suggesting that a similar metabolic pathway was very likely to happen with formate serving as the electron carrier.

To explore the role of aeMO-AsR in the real world, field samples from rice paddies were then used to perform microcosm incubations mimicking in situ (hyp)oxic conditions. Compared to the setups with no amendment, $^{13}CH_4$ addition significantly increased the total $^{13}CO_2$ content both dissolved in pore waters and emitted into headspace (Figures 5 and S16), demonstrating the activity of aeMO. Occurrence of this process was further supported by the high transcriptions of *pmoA* during the microcosm incubations (Figure S17). Meanwhile, the concentrations of inorganic arsenate and arsenite were elevated in pore water samples (Figure S18), while organic arsenic species, that is, DMAs(V) and MMAs(V), were undetectable or at trace concentrations, in accordance with previous studies.[14,79]

Partial release of soil-associated arsenic species could be caused by the abiotic dissolution of iron/manganese (oxyhydr)oxides,[80−82] as observed in autoclaved and microbially inactive setups (Figure S19). Indeed, increases of Fe(II), total Fe, and Mn(II) were observed in pore waters over the microcosm incubations, but with no significant differences between setups amended or unamended with $^{13}CH_4$ (Figure S20), supporting the abiotic release of arsenite and arsenate. However, setups active in aeMO discharged much more arsenite than ones without $^{13}CH_4$ addition (Figure 5), suggesting that the increased portion of dissolved arsenite should be driven by methane oxidation directly or indirectly.

Given the existence of indigenous and methane-derived organic matters, iron/manganese minerals could be reductively dissolved by microorganisms, leading to a non-selective release of adsorbed arsenate and arsenite.[9,13,78] This was supported by the observed increases in Fe(II) and Mn(II) (Figure S20), as well as in both inorganic arsenic species, in pore waters (Figure S18). Nevertheless, all the soluble substances measured above, except for arsenite, showed no remarkable difference between setups with and without $^{13}CH_4$ addition, illustrating a negligible contribution to the aeMO-induced arsenite release by iron/manganese reductive dissolution. We therefore proposed that the increased portion of dissolved arsenite in the presence of aeMO indeed resulted from arsenate reduction, which was further confirmed by the high transcriptional activity of the key gene *arrA* (Figure S17). Taken together, all these results support our initial hypothesis that aeMO could directly be coupled to the reduction of soil-bound arsenate and release the resulting arsenite into solution. Based on such microcosm incubations of soil samples, we estimated that in the top layer of the soils where oxygen was present, aeMO-AsR contributed on average 50.0% (16.8–76.2%, $n = 6$) to the total soil-arsenic mobilization (Table S3, see detailed calculations in the Methods section), suggesting that this newly discovered bioprocess was a previously overlooked yet very important pathway for releasing arsenic from soils and may have a broad impact on biogeochemical arsenic cycling associated with environmental health.

Global Distribution of the Newly Discovered aeMO-AsR. Thermodynamic calculations suggested that methane oxidation to formate was energetically favorable in nature, although under extremely low concentrations of methane and oxygen (Figure 6a). Formate at a concentration as low as 10 μM, as measured in this study, would be sufficient to drive arsenate reduction and generate energy for microorganisms (i.e., $\Delta G = -104.21$ kJ/mol^{-1} As) in arsenate-laden environments (Figure 6b). Taken together, aeMO-AsR mediated by formate can occur in environments where all the necessary substrates are present (Figure 6c). In support of this, the simultaneous presence of *pmoA* and *arrA* was demonstrated in multiple metagenomes sampled from various natural environments (Figure 6d). These habitats included river estuaries, freshwater sediments, and marine waters (Table S4). Some natural environments, such as the Hudson Canyon and Columbia River estuaries,[83,84] were hotspots for aeMO, potentially contributing to active arsenate reduction.

Arsenate reduction is generally considered to be promoted by microbial oxidation of organic acids like acetate and lactate.[9,10,12] Recent findings highlighted the role of methane

https://doi.org/10.1021/acs.est.2c01878
Environ. Sci. Technol. 2022, 56, 11845−11856

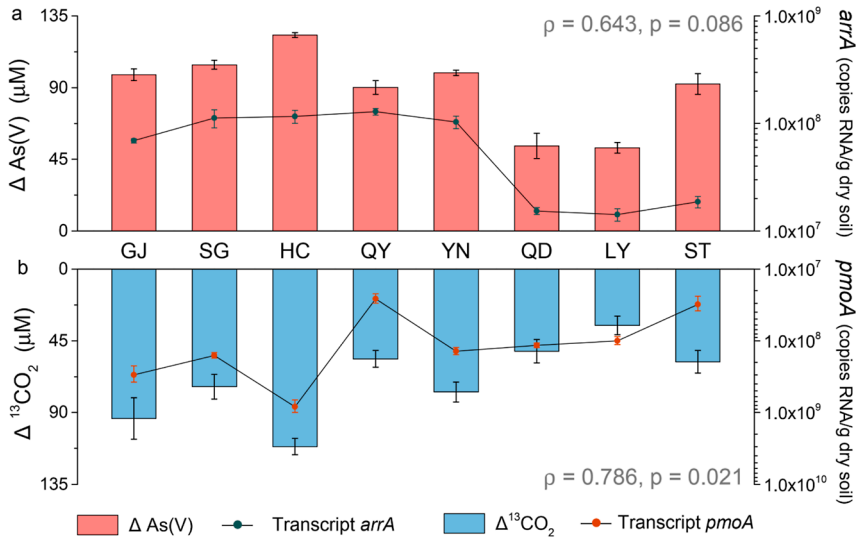

Figure 4. Changes of As(V) and $^{13}CO_2$ concentrations during 5-day incubations inoculated with soil samples. ΔAs(V) in (a) indicates the difference in arsenate reduction between incubations with $^{13}CH_4$ or argon, while $\Delta^{13}CO_2$ in (b) indicates the difference in $^{13}CO_2$ production with or without the addition of arsenate. Transcriptions of *arrA* and *pmoA* were determined immediately at the end of incubations and shown in the logarithmic axes. Correlations between biochemical processes and gene transcriptions were tested by Spearman rank correlation, where ρ and p indicate the correlation efficiency and statistical probability, respectively. Error bars indicate standard deviations of three replicates.

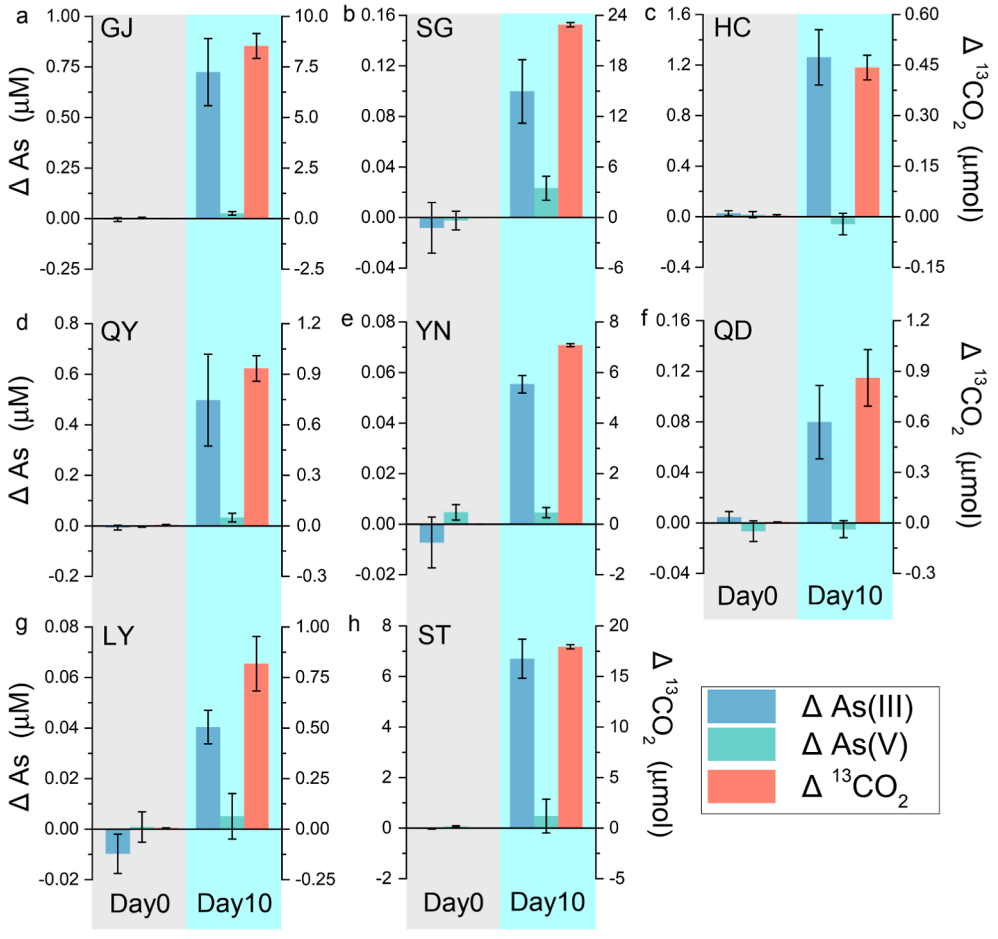

Figure 5. Changes of dissolved arsenic and produced $^{13}CO_2$ during microcosm incubations mimicking in situ conditions. Arsenic was sampled from the pore water, while $^{13}CO_2$ was from both the pore water and the headspace. Δ values indicate the difference in concentrations between incubations amended with $^{13}CH_4$ or argon. Error bars indicate standard deviations of triplicates.

in reducing arsenate under anoxic conditions.[14] Here, we provide the first experimental evidence for methane-dependent arsenate reduction under (hyp)oxic conditions, together advancing our understandings of how methane interacts with

https://doi.org/10.1021/acs.est.2c01878
Environ. Sci. Technol. 2022, 56, 11845−11856

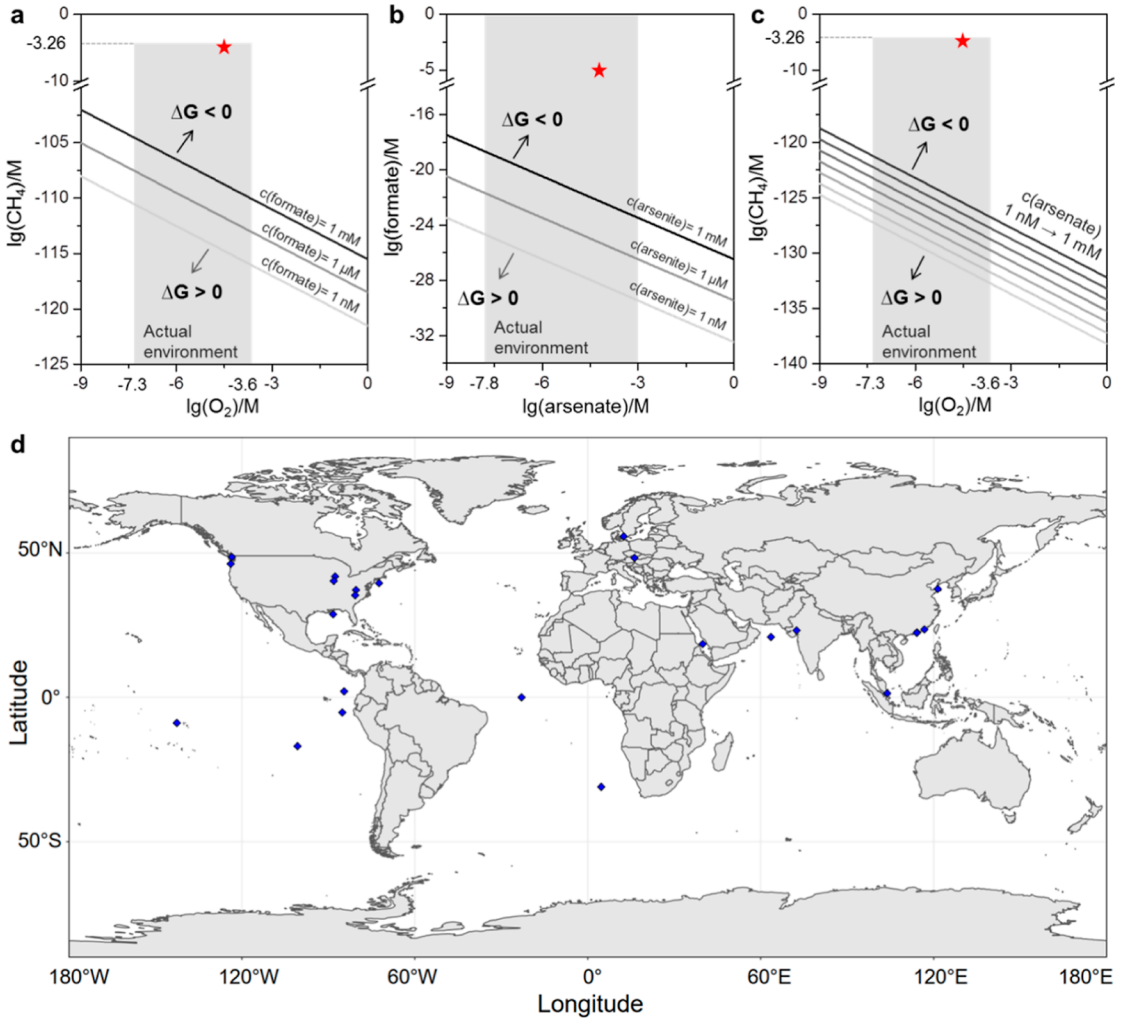

Figure 6. Thermodynamic favorability and global distribution of aeMO-AsR. (a–c) Thermodynamics of the three reactions $CH_4 + 1.5O_2 = HCOO^- + H_2O + H^+$, $HAsO_4^{2-} + HCOO^- + 2H^+ = H_3AsO_3 + HCO_3^-$, and $HAsO_4^{2-} + CH_4 + 1.5O_2 + H^+ = H_3AsO_3 + HCO_3^- + H_2O$ (eqs 4–6) under different conditions, respectively. Thick lines represent the curves for $\Delta G = 0$ with defined concentrations of reactant or product species, for example, c(formate) = 1 mM for the black line (a). $\Delta G < 0$ or $\Delta G > 0$, as indicated by arrows, suggest that the reaction is either thermodynamically favorable or not. The experimental condition is indicated by red stars. (d) Geographic location of natural environmental samples that contain both *pmoA* and *arrA* genes (blue diamonds), extracted from the non-redundant protein database of MGnify. Detailed geographic information can be found in Table S4.

arsenate along the entire oxygen gradient (Figure S21). In the case of unavailable oxygen, AOM outcompetes aerobic oxidation of methane, while this relation is reversed in the presence of oxygen, to fuel arsenate reduction. Given that the reduction product arsenite has greater toxicity and bioavailability, arsenate reduction driven by both anaerobic and aerobic oxidation of methane would release arsenic originally associated with solids into aquatic environments and thus pose more threats to ecosystem health. Overall, our discovery presented here not only reveals the contribution of methane to reductive arsenic mobilization but also highlights an additional ecological impact of this important greenhouse gas on environmental health in addition to its well-recognized climate warming effect.

■ ASSOCIATED CONTENT

Supporting Information

The Supporting Information is available free of charge at https://pubs.acs.org/doi/10.1021/acs.est.2c01878.

Schematic of two incubation methods for field samples; arsenate reduction dynamics in a CH_4-fed bioreactor; scanning electron micrograph and energy-dispersive X-ray spectrum of the bulk deposits; arsenate concentration over time in the enrichment culture devoid of methane; arsenate concentration in batch setups under different conditions; taxonomy and relative abundance of quality-controlled metagenomic sequence reads; phylogeny of the recovered MAGs; phylogenetic tree of the particulate MMO alpha subunit; changes of transcript abundances under different conditions; changes in gene abundances of batch incubations dependent on different conditions; phylogenetic tree of the anaerobic arsenite oxidase beta subunit (ArxB) and the respiratory arsenate reductase beta subunit (ArrB); alignment of the proposed arsenate reductase catalytic subunit encoded in Bin.64 with the characterized counterparts; arsenate reduction in incubations of the enrichment culture amended with methane (0.09 mmol) or formate (3.6 mmol); phylogenetic tree of the formate

https://doi.org/10.1021/acs.est.2c01878
Environ. Sci. Technol. 2022, 56, 11845–11856

dehydrogenase alpha subunit; reduced As(V) and produced $^{13}CO_2$ in 5-day incubations inoculated by soil samples; concentrations of total $^{13}CO_2$ in the microcosm incubations; transcriptions of *arrA* and *pmoA* in the soil microcosm incubations mimicking in situ conditions; concentrations of As(V) and As(III) in the pore waters in the microcosm incubations; changes of arsenic concentrations in the pore waters in the microcosm incubations; concentration changes of Fe and Mn species in the pore waters in the microcosm incubations; and conceptual diagram of methane oxidation coupled to arsenate reduction in nature (PDF)

Information of field samples used in this study; genome quality and assigned taxonomy of MAGs; contributions to arsenite release based on microcosm incubations; and geographical information on bio-informatic predicted samples (XLSX)

AUTHOR INFORMATION

Corresponding Author

He-Ping Zhao − *MOE Key Lab of Environmental Remediation and Ecosystem Health, College of Environmental and Resource Sciences, Zhejiang University, Hangzhou 310058, China;* orcid.org/0000-0002-5177-8010; Phone: 0086-571-88982739; Email: zhaohp@zju.edu.cn

Authors

Ling-Dong Shi − *MOE Key Lab of Environmental Remediation and Ecosystem Health, College of Environmental and Resource Sciences, Zhejiang University, Hangzhou 310058, China*

Yu-Jie Zhou − *MOE Key Lab of Environmental Remediation and Ecosystem Health, College of Environmental and Resource Sciences, Zhejiang University, Hangzhou 310058, China*

Xian-Jin Tang − *MOE Key Lab of Environmental Remediation and Ecosystem Health, College of Environmental and Resource Sciences, Zhejiang University, Hangzhou 310058, China;* orcid.org/0000-0002-7515-2047

Andreas Kappler − *Center for Applied Geosciences, University of Tübingen, Tübingen 72074, Germany;* orcid.org/0000-0002-3558-9500

Ludmila Chistoserdova − *Department of Chemical Engineering, University of Washington, Seattle, Washington 98195-0005, United States*

Li-Zhong Zhu − *MOE Key Lab of Environmental Remediation and Ecosystem Health, College of Environmental and Resource Sciences, Zhejiang University, Hangzhou 310058, China;* orcid.org/0000-0001-5044-277X

Complete contact information is available at: https://pubs.acs.org/10.1021/acs.est.2c01878

Notes

The authors declare no competing financial interest.

ACKNOWLEDGMENTS

The authors greatly thank the "National Natural Science Foundation of China (grant nos. 32061133002, 51878596, and NSF22193061)", the "National Key Technology R&D Program (2018YFC1802203)", and the "Key Technology R&D Program of Zhejiang Province (2021C03171, 2020C03011)" for their financial support. The authors very much appreciate Prof. Fang-Jie Zhao from Nanjing Agricultural University, Prof. Zi-Jun Wu from Tongji University, and Prof. Ping Li from China University of Geosciences (Beijing) for donating field samples. The authors also thank Prof. Yong-Guan Zhu and Dr. Xiyang Dong for discussing the results and assisting in manuscript preparation. The author L.-D.S. would like to thank the support from Shanghai Tongji Gao Tingyao Environmental Science and Technology Development Foundation.

REFERENCES

(1) Cullen, W. R.; Reimer, K. J. Arsenic Speciation in the Environment. *Chem. Rev.* **1989**, *89*, 713−764.

(2) Berg, M.; Tran, H. C.; Nguyen, T. C.; Pham, H. V.; Schertenleib, R.; Giger, W. Arsenic contamination of groundwater and drinking water in Vietnam: A human health threat. *Environ. Sci. Technol.* **2001**, *35*, 2621−2626.

(3) Fendorf, S.; Michael, H. A.; van Geen, A. Spatial and Temporal Variations of Groundwater Arsenic in South and Southeast Asia. *Science* **2010**, *328*, 1123−1127.

(4) Zhu, Y. G.; Yoshinaga, M.; Zhao, F. J.; Rosen, B. P. Earth abides arsenic biotransformations. *Annu. Rev. Earth Planet. Sci.* **2014**, *42*, 443−467.

(5) Podgorski, J.; Berg, M. Global threat of arsenic in groundwater. *Science* **2020**, *368*, 845−850.

(6) Islam, F. S.; Gault, A. G.; Boothman, C.; Polya, D. A.; Charnock, J. M.; Chatterjee, D.; Lloyd, J. R. Role of metal-reducing bacteria in arsenic release from Bengal delta sediments. *Nature* **2004**, *430*, 68−71.

(7) Islam, F. S.; Pederick, R. L.; Gault, A. G.; Adams, L. K.; Polya, D. A.; Charnock, J. M.; Lloyd, J. R. Interactions between the Fe(III)-reducing bacterium Geobacter sulfurreducens and arsenate, and capture of the metalloid by biogenic Fe(II). *Appl. Environ. Microbiol.* **2005**, *71*, 8642−8648.

(8) Anawar, H. M.; Akai, J.; Komaki, K.; Terao, H.; Yoshioka, T.; Ishizuka, T.; Safiullah, S.; Kato, K. Geochemical occurrence of arsenic in groundwater of Bangladesh: sources and mobilization processes. *J. Geochem. Explor.* **2003**, *77*, 109−131.

(9) Glodowska, M.; Stopelli, E.; Schneider, M.; Lightfoot, A.; Rathi, B.; Straub, D.; Patzner, M.; Duyen, V. T.; Berg, M.; Kleindienst, S.; Kappler, A.; Members, A. T. Role of in Situ Natural Organic Matter in Mobilizing As during Microbial Reduction of Fe-III-Mineral-Bearing Aquifer Sediments from Hanoi (Vietnam). *Environ. Sci. Technol.* **2020**, *54*, 4149−4159.

(10) Kudo, K.; Yamaguchi, N.; Makino, T.; Ohtsuka, T.; Kimura, K.; Dong, D. T.; Amachi, S. Release of Arsenic from Soil by a Novel Dissimilatory Arsenate-Reducing Bacterium, Anaeromyxobacter sp Strain PSR-1. *Appl. Environ. Microbiol.* **2013**, *79*, 4635−4642.

(11) Qiao, J.; Li, X.; Li, F.; Liu, T.; Young, L. Y.; Huang, W.; Sun, K.; Tong, H.; Hu, M. Humic Substances Facilitate Arsenic Reduction and Release in Flooded Paddy Soil. *Environ. Sci. Technol.* **2019**, *53*, 5034−5042.

(12) Qiao, J. T.; Li, X. M.; Hu, M.; Li, F. B.; Young, L. Y.; Sun, W. M.; Huang, W. L.; Cui, J. H. Transcriptional Activity of Arsenic-Reducing Bacteria and Genes Regulated by Lactate and Biochar during Arsenic Transformation in Flooded Paddy Soil. *Environ. Sci. Technol.* **2018**, *52*, 61−70.

(13) Zobrist, J.; Dowdle, P. R.; Davis, J. A.; Oremland, R. S. Mobilization of arsenite by dissimilatory reduction of adsorbed arsenate. *Environ. Sci. Technol.* **2000**, *34*, 4747−4753.

(14) Shi, L. D.; Guo, T.; Lv, P. L.; Niu, Z. F.; Zhou, Y. J.; Tang, X. J.; Zheng, P.; Zhu, L. Z.; Zhu, Y. G.; Kappler, A.; Zhao, H. P. Coupled anaerobic methane oxidation and reductive arsenic mobilization in wetland soils. *Nat. Geosci.* **2020**, *13*, 799−805.

(15) Glodowska, M.; Stopelli, E.; Stopelli, M.; Schneider, B.; Rathi, D.; Straub, A.; Lightfoot, R.; Kipfer, M.; Berg, M.; Jetten, S.;

Kleindienst, A.; Kappler, A. Arsenic mobilization by anaerobic iron-dependent methane oxidation. *Commun. Earth Environ.* **2020**, *1*, 42.
(16) Glodowska, M.; Stopelli, E.; Straub, D.; Vu Thi, D.; Trang, P. T. K.; Viet, P. H.; AdvectAs team members, m.; Berg, M.; Kappler, A.; Kleindienst, S. Arsenic behavior in groundwater in Hanoi (Vietnam) influenced by a complex biogeochemical network of iron, methane, and sulfur cycling. *J. Hazard. Mater.* **2021**, *407*, 124398.
(17) Winograd, I. J.; Robertson, F. N. Deep Oxygenated Ground Water: anomaly or common occurrence? *Science* **1982**, *216*, 1227−1230.
(18) Chistoserdova, L.; Kalyuzhnaya, M. G.; Lidstrom, M. E. The Expanding World of Methylotrophic Metabolism. *Annu. Rev. Microbiol.* **2009**, *63*, 477−499.
(19) Semrau, J. D.; DiSpirito, A. A.; Gu, W.; Yoon, S. Metals and Methanotrophy. *Appl. Environ. Microbiol.* **2018**, *84*, No. e02289.
(20) Balasubramanian, R.; Smith, S. M.; Rawat, S.; Yatsunyk, L. A.; Stemmler, T. L.; Rosenzweig, A. C. Oxidation of methane by a biological dicopper centre. *Nature* **2010**, *465*, 115−119.
(21) Ross, M. O.; MacMillan, F.; Wang, J. Z.; Nisthal, A.; Lawton, T. J.; Olafson, B. D.; Mayo, S. L.; Rosenzweig, A. C.; Hoffman, B. M. Particulate methane monooxygenase contains only mononuclear copper centers. *Science* **2019**, *364*, 566−570.
(22) Kits, K. D.; Klotz, M. G.; Stein, L. Y. Methane oxidation coupled to nitrate reduction under hypoxia by the Gammaproteobacterium Methylomonas denitrificans, sp. nov. type strain FJG1. *Environ. Microbiol.* **2015**, *17*, 3219−3232.
(23) Modin, O.; Fukushi, K.; Nakajima, F.; Yamamoto, K. Nitrate removal and biofilm characteristics in methanotrophic membrane biofilm reactors with various gas supply regimes. *Water Res.* **2010**, *44*, 85−96.
(24) Naqvi, S. W. A.; Lam, P.; Narvenkar, G.; Sarkar, A.; Naik, H.; Pratihary, A.; Shenoy, D. M.; Gauns, M.; Kurian, S.; Damare, S.; Duret, M.; Lavik, G.; Kuypers, M. M. M. Methane stimulates massive nitrogen loss from freshwater reservoirs in India. *Nat. Commun.* **2018**, *9*, 1265.
(25) Enbaia, S.; Eswayah, A.; Hondow, N.; Gardiner, P. H. E.; Smith, T. J. Detoxification, active uptake, and intracellular accumulation of chromium species by a methane-oxidizing bacterium. *Appl. Environ. Microbiol.* **2021**, *87*, No. e00947.
(26) Zheng, Y.; Wang, H.; Liu, Y.; Zhu, B.; Li, J.; Yang, Y.; Qin, W.; Chen, L.; Wu, X.; Chistoserdova, L.; Zhao, F. Methane-dependent mineral reduction by aerobic methanotrophs under hypoxia. *Environ. Sci. Technol. Lett.* **2020**, *7*, 606−612.
(27) Kalyuzhnaya, M. G.; Yang, S.; Rozova, O. N.; Smalley, N. E.; Clubb, J.; Lamb, A.; Gowda, G. A. N.; Raftery, D.; Fu, Y.; Bringel, F.; Vuilleumier, S.; Beck, D. A. C.; Trotsenko, Y. A.; Khmelenina, V. N.; Lidstrom, M. E. Highly efficient methane biocatalysis revealed in a methanotrophic bacterium. *Nat. Commun.* **2013**, *4*, 2785.
(28) Zhu, J.; Wang, Q.; Yuan, M. D.; Tan, G. Y. A.; Sun, F. Q.; Wang, C.; Wu, W. X.; Lee, P. H. Microbiology and potential applications of aerobic methane oxidation coupled to denitrification (AME-D) process: A review. *Water Res.* **2016**, *90*, 203−215.
(29) Gilman, A.; Fu, Y. F.; Hendershott, M.; Chu, F.; Puri, A. W.; Smith, A. L.; Pesesky, M.; Lieberman, R.; Beck, D. A. C.; Lidstrom, M. E. Oxygen-limited metabolism in the methanotroph Methylomicrobium buryatense 5GB1C. *Peerj* **2017**, *5*, No. e3945.
(30) Nordstrom, D. K.; Majzlan, J.; Konigsberger, E. Thermodynamic Properties for Arsenic Minerals and Aqueous Species. *Rev. Mineral. Geochem.* **2014**, *79*, 217−255.
(31) Lai, C. Y.; Dong, Q. Y.; Rittmann, B. E.; Zhao, H. P. Bioreduction of antimonate by anaerobic methane oxidation in a membrane biofilm batch reactor. *Environ. Sci. Technol.* **2018**, *52*, 8693−8700.
(32) Luo, Y. H.; Chen, R.; Wen, L. L.; Meng, F.; Zhang, Y.; Lai, C. Y.; Rittmann, B. E.; Zhao, H. P.; Zheng, P. Complete perchlorate reduction using methane as the sole electron donor and carbon source. *Environ. Sci. Technol.* **2015**, *49*, 2341−2349.
(33) Prior, S. D.; Dalton, H. Acetylene as a Suicide Substrate and Active-Site Probe for Methane Monooxygenase from Methylococcus-Capsulatus (Bath). *FEMS Microbiol. Lett.* **1985**, *29*, 105−109.
(34) Oremland, R. S.; Capone, D. G. Use of "Specific" Inhibitors in Biogeochemistry and Microbial Ecology. *Adv. Microb. Ecol.* **1988**, *10*, 285−383.
(35) Hoehler, T. M.; Alperin, M. J.; Albert, D. B.; Martens, C. S. Field and Laboratory Studies of Methane Oxidation in an Anoxic Marine Sediment - Evidence for a Methanogen-Sulfate Reducer Consortium. *Global Biogeochem. Cycles* **1994**, *8*, 451−463.
(36) Bao, S. D. *Soil Agrochemical Analysis*, 3rd ed. 2011, China Agricultural Press, (pp 495), p 135.
(37) Shi, L. D.; Lv, P. L.; Wang, M.; Lai, C. Y.; Zhao, H. P. A mixed consortium of methanotrophic archaea and bacteria boosts methane -dependent selenate reduction. *Sci. Total Environ.* **2020**, *732*, 139310.
(38) Maeda, H.; Fujimoto, C.; Haruki, Y.; Maeda, T.; Kokeguchi, S.; Petelin, M.; Arai, H.; Tanimoto, I.; Nishimura, F.; Takashiba, S. Quantitative real-time PCR using TaqMan and SYBR Green for Actinobacillus actinomycetemcomitans, Porphyromonas gingivalis, Prevotella intermedia, tetQ gene and total bacteria. *FEMS Immunol. Med. Microbiol.* **2003**, *39*, 81−86.
(39) Mirza, B. S.; Sorensen, D. L.; Dupont, R. R.; McLean, J. E. New Arsenate Reductase Gene (arrA) PCR Primers for Diversity Assessment and Quantification in Environmental Samples. *Appl. Environ. Microbiol.* **2017**, *83*, No. e02725.
(40) Paszczynski, A. J.; Paidisetti, R.; Johnson, A. K.; Crawford, R. L.; Colwell, F. S.; Green, T.; Delwiche, M.; Lee, H.; Newby, D.; Brodie, E. L.; Conrad, M. Proteomic and targeted qPCR analyses of subsurface microbial communities for presence of methane monooxygenase. *Biodegradation* **2011**, *22*, 1045−1059.
(41) Bolger, A. M.; Lohse, M.; Usadel, B. Trimmomatic: a flexible trimmer for Illumina sequence data. *Bioinformatics* **2014**, *30*, 2114−2120.
(42) Menzel, P.; Ng, K. L.; Krogh, A. Fast and sensitive taxonomic classification for metagenomics with Kaiju. *Nat. Commun.* **2016**, *7*, 11257.
(43) Nurk, S.; Meleshko, D.; Korobeynikov, A.; Pevzner, P. A. metaSPAdes: a new versatile metagenomic assembler. *Genome Res.* **2017**, *27*, 824−834.
(44) Kang, D. W. D.; Li, F.; Kirton, E.; Thomas, A.; Egan, R.; An, H.; Wang, Z. MetaBAT 2: an adaptive binning algorithm for robust and efficient genome reconstruction from metagenome assemblies. *Peerj* **2019**, *7*, No. e7359.
(45) Parks, D. H.; Imelfort, M.; Skennerton, C. T.; Hugenholtz, P.; Tyson, G. W. CheckM: assessing the quality of microbial genomes recovered from isolates, single cells, and metagenomes. *Genome Res.* **2015**, *25*, 1043−1055.
(46) Parks, D. H.; Chuvochina, M.; Chaumeil, P. A.; Rinke, C.; Mussig, A. J.; Hugenholtz, P. A complete domain-to-species taxonomy for Bacteria and Archaea. *Nat. Biotechnol.* **2020**, *38*, 1079−1086.
(47) Chaumeil, P.-A.; Mussig, A. J.; Hugenholtz, P.; Parks, D. H. GTDB-Tk: a toolkit to classify genomes with the Genome Taxonomy Database. *Bioinformatics* **2019**, *36*, 1925−1927.
(48) Dong, X. L.; Strous, M. An integrated pipeline for annotation and visualization of metagenomic contigs. *Front. Genet.* **2019**, *10*, 999.
(49) Eddy, S. R. Accelerated profile HMM searches. *PLoS Comput. Biol.* **2011**, *7*, No. e1002195.
(50) Edgar, R. C. MUSCLE: multiple sequence alignment with high accuracy and high throughput. *Nucleic Acids Res.* **2004**, *32*, 1792−1797.
(51) Nguyen, L. T.; Schmidt, H. A.; von Haeseler, A.; Minh, B. Q. IQ-TREE: A Fast and Effective Stochastic Algorithm for Estimating Maximum-Likelihood Phylogenies. *Mol. Biol. Evol.* **2015**, *32*, 268−274.
(52) Haft, D. H.; Selengut, J. D.; Richter, R. A.; Harkins, D.; Basu, M. K.; Beck, E. TIGRFAMs and Genome Properties in 2013. *Nucleic Acids Res.* **2013**, *41*, D387−D395.
(53) Finn, R. D.; Bateman, A.; Clements, J.; Coggill, P.; Eberhardt, R. Y.; Eddy, S. R.; Heger, A.; Hetherington, K.; Holm, L.; Mistry, J.;

https://doi.org/10.1021/acs.est.2c01878
Environ. Sci. Technol. 2022, 56, 11845−11856

Sonnhammer, E. L. L.; Tate, J.; Punta, M. Pfam: the protein families database. *Nucleic Acids Res.* **2014**, *42*, D222−D230.
(54) Parks, D. H.; Rinke, C.; Chuvochina, M.; Chaumeil, P. A.; Woodcroft, B. J.; Evans, P. N.; Hugenholtz, P.; Tyson, G. W. Recovery of nearly 8,000 metagenome-assembled genomes substantially expands the tree of life. *Nat. Microbiol.* **2017**, *2*, 1533−1542.
(55) Boratyn, G. M.; Camacho, C.; Cooper, P. S.; Coulouris, G.; Fong, A.; Ma, N.; Madden, T. L.; Matten, W. T.; McGinnis, S. D.; Merezhuk, Y.; Raytselis, Y.; Sayers, E. W.; Tao, T.; Ye, J.; Zaretskaya, I. BLAST: a more efficient report with usability improvements. *Nucleic Acids Res.* **2013**, *41*, W29−W33.
(56) Kanehisa, M.; Sato, Y.; Morishima, K. BlastKOALA and GhostKOALA: KEGG Tools for Functional Characterization of Genome and Metagenome Sequences. *J. Mol. Biol.* **2016**, *428*, 726−731.
(57) Lu, S. N.; Wang, J. Y.; Chitsaz, F.; Derbyshire, M. K.; Geer, R. C.; Gonzales, N. R.; Gwadz, M.; Hurwitz, D. I.; Marchler, G. H.; Song, J. S.; Thanki, N.; Yamashita, R. A.; Yang, M. Z.; Zhang, D. C.; Zheng, C. J.; Lanczycki, C. J.; Marchler-Bauer, A. CDD/SPARCLE: the conserved domain database in 2020. *Nucleic Acids Res.* **2020**, *48*, D265−D268.
(58) Kelley, L. A.; Mezulis, S.; Yates, C. M.; Wass, M. N.; Sternberg, M. J. The Phyre2 web portal for protein modeling, prediction and analysis. *Nat. Protoc.* **2015**, *10*, 845−858.
(59) Lide, D. R. *CRC Handbook of Chemistry and Physics*; CRC press, 2004; Vol. *85*.
(60) Dolfing, J. *Hydrocarbon and Lipid Microbiology Protocols*; McGenity, T. J., et al., Eds.; Springer: Berlin, Heidelberg, 2015; pp 155−163.
(61) Ruff, S. E.; Kuhfuss, H.; Wegener, G.; Lott, C.; Ramette, A.; Wiedling, J.; Knittel, K.; Weber, M. Methane Seep in Shallow-Water Permeable Sediment Harbors High Diversity of Anaerobic Methanotrophic Communities, Elba, Italy. *Front. Microbiol.* **2016**, *7*, 374.
(62) WHO World Health Organization. *Environmental Health Criteria 224: Arsenic and Arsenic Compounds*, 2004.
(63) Luo, W. T.; Gao, X. B.; Zhang, X. Geochemical processes controlling the groundwater chemistry and fluoride contamination in the Yuncheng Basin, China-An area with complex hydrogeochemical conditions. *PLoS One* **2018**, *13*, No. e0199082.
(64) Buchfink, B.; Xie, C.; Huson, D. H. Fast and sensitive protein alignment using DIAMOND. *Nat. Methods* **2015**, *12*, 59−60.
(65) Mitchell, A. L.; Almeida, A.; Beracochea, M.; Boland, M.; Burgin, J.; Cochrane, G.; Crusoe, M. R.; Kale, V.; Potter, S. C.; Richardson, L. J.; Sakharova, E.; Scheremetjew, M.; Korobeynikov, A.; Shlemov, A.; Kunyavskaya, O.; Lapidus, A.; Finn, R. D. MGnify: the microbiome analysis resource in 2020. *Nucleic Acids Res.* **2020**, *48*, D570−D578.
(66) Shi, L. D.; Wang, M.; Han, Y. L.; Lai, C. Y.; Shapleigh, J. P.; Zhao, H. P. Multi-omics reveal various potential antimonate reductases from phylogenetically diverse microorganisms. *Appl. Microbiol. Biotechnol.* **2019**, *103*, 9119−9129.
(67) Ettwig, K. F.; Butler, M. K.; Le Paslier, D.; Pelletier, E.; Mangenot, S.; Kuypers, M. M.; Schreiber, F.; Dutilh, B. E.; Zedelius, J.; de Beer, D.; Gloerich, J.; Wessels, H. J.; van Alen, T.; Luesken, F.; Wu, M. L.; van de Pas-Schoonen, K. T.; Op den Camp, H. J.; Janssen-Megens, E. M.; Francoijs, K. J.; Stunnenberg, H.; Weissenbach, J.; Jetten, M. S.; Strous, M. Nitrite-driven anaerobic methane oxidation by oxygenic bacteria. *Nature* **2010**, *464*, 543−548.
(68) Ettwig, K. F.; Shima, S.; van de Pas-Schoonen, K. T.; Kahnt, J.; Medema, M. H.; op den Camp, H. J. M.; Jetten, M. S. M.; Strous, M. Denitrifying bacteria anaerobically oxidize methane in the absence of Archaea. *Environ. Microbiol.* **2008**, *10*, 3164−3173.
(69) Culpepper, M. A.; Cutsail, G. E.; Hoffman, B. M.; Rosenzweig, A. C. Evidence for Oxygen Binding at the Active Site of Particulate Methane Monooxygenase. *J. Am. Chem. Soc.* **2012**, *134*, 7640−7643.
(70) Shi, L.-D.; Wang, M.; Li, Z.-Y.; Lai, C.-Y.; Zhao, H.-P. Dissolved oxygen has no inhibition on methane oxidation coupled to selenate reduction in a membrane biofilm reactor. *Chemosphere* **2019**, *234*, 855−863.
(71) Chen, J. W.; Strous, M. Denitrification and aerobic respiration, hybrid electron transport chains and co-evolution. *Biochim. Biophys. Acta, Bioenerg.* **2013**, *1827*, 136−144.
(72) Zhu, Y. G.; Xue, X. M.; Kappler, A.; Rosen, B. P.; Meharg, A. A. Linking genes to microbial biogeochemical cycling: lessons from arsenic. *Environ. Sci. Technol.* **2017**, *51*, 7326−7339.
(73) Glasser, N. R.; Oyala, P. H.; Osborne, T. H.; Santini, J. M.; Newman, D. K. Structural and mechanistic analysis of the arsenate respiratory reductase provides insight into environmental arsenic transformations. *Proc. Natl. Acad. Sci. U.S.A.* **2018**, *115*, E8614−E8623.
(74) Montag, D.; Schink, B. Formate and Hydrogen as Electron Shuttles in Terminal Fermentations in an Oligotrophic Freshwater Lake Sediment. *Appl. Environ. Microbiol.* **2018**, *84*, No. e01572.
(75) Sieber, J. R.; Le, H. M.; McInerney, M. J. The importance of hydrogen and formate transfer for syntrophic fatty, aromatic and alicyclic metabolism. *Environ. Microbiol.* **2014**, *16*, 177−188.
(76) Thiele, J. H.; Zeikus, J. G. Control of Interspecies Electron Flow during Anaerobic-Digestion - Significance of Formate Transfer Versus Hydrogen Transfer during Syntrophic Methanogenesis in Flocs. *Appl. Environ. Microbiol.* **1988**, *54*, 20−29.
(77) Shi, L.-D.; Lv, P.-L.; McIlroy, S. J.; Wang, Z.; Dong, X.-L.; Kouris, A.; Lai, C.-Y.; Tyson, G. W.; Strous, M.; Zhao, H.-P. Methane-dependent selenate reduction by a bacterial consortium. *ISME Journal* **2021**, *15*, 3683−3692.
(78) Jiang, J.; Bauer, I.; Paul, A.; Kappler, A. Arsenic redox changes by microbially and chemically formed semiquinone radicals and hydroquinones in a humic substance model quinone. *Environ. Sci. Technol.* **2009**, *43*, 3639−3645.
(79) Jia, Y.; Huang, H.; Zhong, M.; Wang, F. H.; Zhang, L. M.; Zhu, Y. G. Microbial arsenic methylation in soil and rice rhizosphere. *Environ. Sci. Technol.* **2013**, *47*, 3141−3148.
(80) Dixit, S.; Hering, J. G. Comparison of arsenic(V) and arsenic(III) sorption onto iron oxide minerals: Implications for arsenic mobility. *Environ. Sci. Technol.* **2003**, *37*, 4182−4189.
(81) Manning, B. A.; Fendorf, S. E.; Bostick, B.; Suarez, D. L. Arsenic(III) oxidation and arsenic(V) adsorption reactions on synthetic birnessite. *Environ. Sci. Technol.* **2002**, *36*, 976−981.
(82) Chiu, V. Q.; Hering, J. G. Arsenic adsorption and oxidation at manganite surfaces. 1. Method for simultaneous determination of adsorbed and dissolved arsenic species. *Environ. Sci. Technol.* **2000**, *34*, 2029−2034.
(83) Leonte, M.; Kessler, J. D.; Kellermann, M. Y.; Arrington, E. C.; Valentine, D. L.; Sylva, S. P. Rapid rates of aerobic methane oxidation at the feather edge of gas hydrate stability in the waters of Hudson Canyon, US Atlantic Margin. *Geochim. Cosmochim. Acta* **2017**, *204*, 375−387.
(84) Pfeiffer-Herbert, A. S.; Prahl, F. G.; Hales, B.; Lerczak, J. A.; Pierce, S. D.; Levine, M. D. High resolution sampling of methane transport in the Columbia River near-field plume: Implications for sources and sinks in a river-dominated estuary. *Limnol. Oceanogr.* **2016**, *61*, S204−S220.

https://doi.org/10.1021/acs.est.2c01878
Environ. Sci. Technol. 2022, 56, 11845−11856